Precipitation distributions for explicit versus parameterized convection in a large-domain high-resolution tropical case study

RMetS
Royal Meteorological Society

Precipitation distributions for explicit versus parametrized convection in a large-domain high-resolution tropical case study

C. E. Holloway,[a]* S. J. Woolnough[a] and G. M. S. Lister[b]
[a]*NCAS–Climate, Department of Meteorology, University of Reading, Reading, UK*
[b]*NCAS–CMS, Department of Meteorology, University of Reading, Reading, UK*

*Correspondence to: C. E. Holloway, Department of Meteorology, University of Reading, Reading, Berkshire, RG6 6BB, UK. E-mail: c.e.holloway@reading.ac.uk

Global climate and weather models tend to produce rainfall that is too light and too regular over the tropical ocean. This is likely because of convective parametrizations, but the problem is not well understood. Here, distributions of precipitation rates are analyzed for high-resolution UK Met Office Unified Model simulations of a 10 day case study over a large tropical domain (∼20°S–20°N and 42°E–180°E). Simulations with 12 km grid length and parametrized convection have too many occurrences of light rain and too few of heavier rain when interpolated onto a 1° grid and compared with Tropical Rainfall Measuring Mission (TRMM) data. In fact, this version of the model appears to have a preferred scale of rainfall around 0.4 mm h^{-1} (10 mm day^{-1}), unlike observations of tropical rainfall. On the other hand, 4 km grid length simulations with explicit convection produce distributions much more similar to TRMM observations. The apparent preferred scale at lighter rain rates seems to be a feature of the convective parametrization rather than the coarse resolution, as demonstrated by results from 12 km simulations with explicit convection and 40 km simulations with parametrized convection. In fact, coarser resolution models with explicit convection tend to have even more heavy rain than observed. Implications for models using convective parametrizations, including interactions of heating and moistening profiles with larger scales, are discussed. One important implication is that the explicit convection 4 km model has temperature and moisture tendencies that favour transitions in the convective regime. Also, the 12 km parametrized convection model produces a more stable temperature profile at its extreme high-precipitation range, which may reduce the chance of very heavy rainfall. Further study is needed to determine whether unrealistic precipitation distributions are due to some fundamental limitation of convective parametrizations or whether parametrizations can be improved, in order to better simulate these distributions. **Copyright © 2012 Royal Meteorological Society**

Key Words: GCM; CRM; CSRM; rainfall; TRMM; cascade

Received 8 August 2011; Revised 12 January 2012; Accepted 23 January 2012; Published online in Wiley Online Library 1 March 2012

Citation: Holloway CE, Woolnough SJ, Lister GMS. 2012. Precipitation distributions for explicit versus parametrized convection in a large-domain high-resolution tropical case study. *Q. J. R. Meteorol. Soc.* **138**: 1692–1708. DOI:10.1002/qj.1903

1. Introduction

Global climate models still have difficulty in simulating tropical climate, specifically rainfall (and associated circulation) patterns at many time scales ranging from interannual to diurnal. These simulated patterns are especially sensitive to details of convective parametrizations, which are used to approximate the cumulative effects of small-scale convection using information at the scale of the model grid cell (Slingo *et al.*, 1996; Lin *et al.*, 2006; Chen *et al.*, 2007; Guilyardi *et al.*, 2009; Turner and Slingo, 2009). Recent advances in computer power are beginning to allow atmospheric simulations large enough to represent large-scale tropical variability while explicitly simulating vertical motions associated with deep convection, thereby sidestepping the need to parametrize tropical rainfall. However, these large-domain high-resolution simulations are still too coarse to resolve convective clouds and motions properly at their observed scales, and they make many assumptions about unresolved processes at even smaller scales. It is vital to compare these simulations with both observations and lower-resolution models using parametrized convection in order to plan future modelling experiments, gain insights for improving parametrizations and improve our understanding of the climate system.

Many studies have shown that convective parametrizations generally lead to rainfall occurring at rates that are too small and over durations that are too long (Dai and Trenberth, 2004; Sun *et al.*, 2006; Stephens *et al.*, 2010), though there have been efforts to improve this behaviour (Wilcox and Donner, 2007). Observations over tropical regions show roughly power-law behaviour of precipitation distributions at lower rain rates, with faster, exponential decreases as very high rain rates are approached (DeMott *et al.*, 2007; Field and Shutts, 2009; Peters *et al.*, 2010). In this article, we compare different runs of the same model over different horizontal resolutions with both parametrized and explicit convection for a real case over a large domain covering the tropical Indian and Western Pacific oceans. We can then compare the model runs with observational data for the same case.

We compare the different models and observations averaged at a common grid spacing of 1° latitude/longitude and time interval of three hours in order to see how convective processes, either explicitly represented or parametrized, affect larger scales. Our hypothesis is that parametrizations, because of weaknesses in their representation of interactions between the convective plume scale and larger scales, will have deficiencies in representing large-scale convective organization and the statistics of precipitation in convective regions. We hope that understanding differences between parametrized and explicit convection will help lead to insights into improving parametrized convection so that it better reflects observations. This would benefit studies of present and future climate, for instance in narrowing climate-model predictions of future changes in precipitation extremes (O'Gorman and Schneider, 2009; Allan *et al.*, 2010).

At the same time, we know of very few studies that use cloud-system-resolving models (CSRMs) for real case studies of tropical convection, especially over large domains. A few case studies using the Nonhydrostatic ICosahedral Atmospheric Model (NICAM) on the Earth Simulator at resolutions as fine as 3.5 km, but more often at 7 km or 14 km, have shown large improvements of tropical phenomena such as the Madden–Julian Oscillation (MJO: Miura *et al.*, 2007; Liu *et al.*, 2009) and tropical cyclones (Oouchi *et al.*, 2009; Taniguchi *et al.*, 2010) compared with coarser resolution simulations. Since high-resolution models with explicit convection will undoubtedly be used more and more for weather prediction and climate studies on global scales, it is vital that these models are systematically tested and studied both to improve their representations of atmospheric processes and to inform our understanding of those processes and the physical mechanisms underlying them.

The simulations discussed in this article have been run and analyzed as part of 'Cascade', a UK consortium project funded by the Natural Environment Research Council (NERC). Cascade seeks to better understand the interaction between tropical convection at the cloud-system scale and larger-scale processes including the MJO, the diurnal cycle of convection over land (Pearson *et al.*, 2010; Love *et al.*, 2011), easterly waves and equatorially trapped waves. To achieve this goal, Cascade employs high-resolution CSRM simulations of the UK Met Office Unified Model (UM) over very large tropical domains and compares them with high-resolution observations, operational analyses provided for the Year of Tropical Convection (YOTC: Waliser and Moncrieff, 2008) and simulations of the same model using parametrized convection.

We describe the observational data and operational analyses in section 2 and explain the set-up of the model simulations in section 3. In section 4 we discuss the mean precipitation over the whole domain and time period of the case study and then present an analysis of probability density distributions of precipitation for the different simulations and observations. In section 5 we present analysis of environmental conditions and heating and moistening rates conditionally averaged by rain rate to explore possible reasons for differences in precipitation distributions. We then discuss these possible mechanisms and the implications of differences in precipitation distributions for the representation of tropical waves and circulation in section 6, before ending with a summary in section 7.

2. Data

We use Tropical Rainfall Measuring Mission (TRMM) 3B42 merged satellite rainfall data, with 0.25° latitude/longitude resolution and three-hour temporal resolution (Huffman *et al.*, 2007). Unless otherwise noted, we restrict our analyses to points over the sea, which include over 80% of the total domain, to avoid more-complex behaviour over land (land points for all data analysis are defined as 1° grid boxes that contain more than 10% of land area as defined by the 4 km model land–sea mask). Because TRMM does not measure very small rain rates well (Huffman *et al.*, 2007), we set any values of rainfall in both the observations and the model data (after being averaged on to the same 1° three-hour grid) that are below 0.04167 mm h^{-1} (1 mm day^{-1}) to zero when we calculate probability densities and fractional contributions to rainfall in section 4.2. However, for the saturation deficit composite on rain rates in section 5.1 we do use lower rain rates for TRMM to represent nearly suppressed conditions, and therefore those composites on TRMM rainfall rates below the threshold rain rate should be viewed with more caution.

We have used Global Precipitation Climatology Project (GPCP: Huffman *et al.*, 1997) daily average data and Precipitation Estimation from Remotely Sensed Information Using Artificial Neural Networks (PERSIANN: Sorooshian *et al.*, 2000) six-hourly data, averaged over the entire domain for this case-study time period, for comparison with TRMM.

European Centre for Medium-Range Weather Forecasts (ECMWF) operational analyses archived for YOTC are used for comparison with model simulations and also as lateral boundary conditions for the limited-area model runs. The analyses are at approximately 25 km grid spacing in the Tropics and values are output at 6 h intervals. To compare values of saturation deficit with model values and to compare column water vapour values with TMI data as discussed below, we interpolate 1° average specific humidity and temperature data from these forecast analyses to 3 h time intervals.

We use TRMM Microwave Imager (TMI) 0.25° precipitation and column water vapour data (Hilburn and Wentz, 2008) for comparison with TRMM merged data and ECMWF operational analyses. Our results do not change when we calculate the same precipitation distributions in section 4.2 with TMI data (not shown), which should be more accurate when and where it is available, rather than with the TRMM merged data. Although we do not compare other merged satellite datasets with TRMM in this article, except for domain-mean precipitation values, PERSIANN data analyzed in Dai *et al.* (2007) show slightly less-frequent and more-intense daily rainfall than TRMM over this region, which, if also true at smaller time scales, would show even more similarity to explicit convection models and less to the parametrized convection models in this study. We have compared the column water vapour of the ECMWF operational analyses with TMI column water vapour over 3 h means (interpolated from 6 h values for ECMWF) and 1° boxes where TMI data are available in the region over 10 days, and they agree fairly well, with a linear Pearson correlation coefficient of 0.97, a median absolute error of 1.8 mm, a mean absolute error of 2.2 mm and a difference of means (ECMWF − TMI), or bias, of −0.64 mm.

3. Model set-up

We use the limited-area mode of version 7.1 of the Met Office Unified Model (UM; Davies *et al.*, 2005), which is semi-Lagrangian and non-hydrostatic; our limited-area runs are updated at the lateral boundaries by ECMWF operational analyses. The initial conditions also come from an ECMWF operational analysis (except for the UM sea surface temperature (SST) analysis, which is fixed at the initial value). The 40 km and 12 km horizontal grid model runs are updated directly from the ECMWF analyses every 6 h at the lateral boundaries via a 'rim' of 8 model grid points within which the prognostic fields are blended linearly between the interior model domain and the exterior analysis. The 4 km grid runs are updated every 30 min from lateral boundary conditions computed from the 12 km parametrized convection run. The rim points are excluded from the domain for the purposes of scientific analysis. The 12 km domain is approximately 21°S–21°N and 41°E–182°E, but all of the analyses here are performed on the shared domain of 19.625°S–19.375°N and 42.375°E–180.375°E at 1° grid spacing.

Within the rim, prognostic variables from the freely evolving inner domain are nudged toward the specified analysis lateral boundary conditions at the outer edge of the rim, with contributions from the two sources weighted linearly across the 8 points so that in the middle of the rim the two sides are weighted equally. This means that the lateral boundary conditions seen by the model at the outer edge of its interior domain partly depend on that domain itself, so that there can be feedback in which, for instance, greater low-level convergence and upper-level divergence in the model interior lead to greater low-level inflow and upper-level outflow in the rim itself and allow for greater moisture convergence and ventilation, which can help to sustain more large-scale heating and ascent in the interior. This can lead to different behaviour in different model runs even though they share the same lateral boundary conditions.

In addition to differences in horizontal grid spacing, there are more vertical levels in the 4 km runs (70 levels) than in the 12 km and 40 km runs (38 levels) with the model top around 40 km height in both cases. Vertical spacing between levels ranges from tens of metres in the boundary layer to around 250 m in the free troposphere for the 4 km models and approximately double this for the 12 km and 40 km models. The vertical levels are terrain-following hybrid heights, but for this article we consider profiles only over the sea so that hybrid height should be equivalent to height above sea level. The time step is 5 min for the 12 km *param* and 40 km runs, 75 s for the 12 km *3Dsmag* run and 30 s for the 4 km runs.

The model physics settings differ among the runs as follows: the 12 km *param* model uses a modified Gregory–Rowntree convective parametrization (with convective available potential energy, or CAPE, as the basis for its closure: Gregory and Rowntree, 1990) with a 30 min CAPE relaxation time scale, as well as an adjustment to reduce this at very high vertical velocity in order to prevent grid-point storms. The standard boundary-layer scheme (Lock *et al.*, 2000) is used for vertical subgrid mixing and there is no horizontal subgrid mixing. There is a single-moment mixed-phase microphysics scheme with two components: ice/snow and liquid water (Wilson and Ballard, 1999). The 40 km model has similar physics to the 12 km *param* model, although the convective parametrization closure lacks the vertical velocity adjustment. The 4 km *2Dsmag* model uses a CAPE-limited version of the convective parametrization that asymptotes to the same 30 min CAPE time scale at zero CAPE but has a CAPE time scale that rapidly increases with increasing CAPE, such that for typical tropical values virtually all rainfall is generated explicitly (Roberts, 2003; Lean *et al.*, 2008). This model version uses the standard boundary-layer scheme for vertical subgrid mixing but includes Smagorinsky-type subgrid mixing in the horizontal dimensions. The microphysics scheme now has prognostic rain in addition to the two components in the version above. The 4 km *3Dsmag* model also uses the CAPE-limited convective parametrization but uses Smagorinsky mixing in all three dimensions, including the vertical, and therefore it does not use the boundary-layer scheme. The microphysics settings are the same as those in the other 4 km version. The 12 km *3Dsmag* model uses the CAPE-limited convective parametrization and Smagorinsky mixing in all three dimensions as well; the microphysics settings are the same as those in the 4 km models.

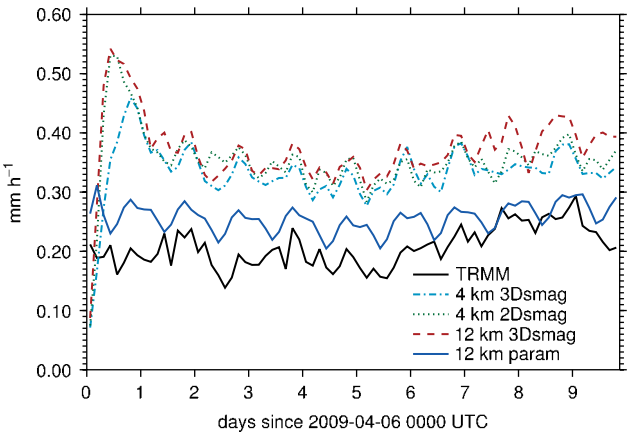

Figure 1. Domain-mean precipitation rates (including land points) in mm h^{-1} for four Cascade runs and TRMM merged precipitation data for 10 days starting on 6 April 2009.

4. Precipitation comparisons

4.1. Mean precipitation

Domain-mean precipitation rate (including land points, which are excluded in later analysis) over the 10 days starting on 6 April 2009 is shown in Figure 1. TRMM observations show little trend over the first five days and then an upward trend in the latter half of the period, with some diurnal-cycle variability evident among other oscillations. Both 4 km model versions have a significantly higher domain-mean precipitation rate than TRMM, whereas the 12 km *param* model (which has parametrized convection) averages only slightly higher than TRMM over the whole domain. The 4 km model versions also exhibit a strong spin-up from almost no precipitation at the start to a very strong maximum and then a partial reduction towards an equilibrium value within the first day. In the 12 km run with explicit convection (12 km *3Dsmag*), the domain-mean precipitation rates are similar to the 4 km runs and even slightly larger. TRMM shows good agreement with two other satellite precipitation products averaged over this domain for this time period: daily-average GPCP and six-hourly PERSIANN both exhibit the same multi-day variability and vary by at most 0.04 mm h^{-1} from TRMM (not shown). Our results are not sensitive to the specific subperiod of time chosen within the case study; the analysis shown and discussed in the rest of the article excludes the first day because of spin-up.

The explicit convection runs likely have more domain-mean rainfall because the explicit convective plumes are wider than typical convective plumes in nature (which usually have cores of a few hundred metres across: LeMone and Zipser, 1980), meaning, at least initially, that there is more build-up of CAPE and also perhaps less lateral fractional entrainment for a given plume. These explicit convection runs are able to maintain this higher domain-mean rainfall despite the same lateral boundary conditions largely because there is feedback between stronger rainfall and the 'circulation' through the outer model rim, as explained above in section 3. We have checked this by comparing the advection of moisture over the whole domain for the 4 km *3Dsmag* model and the 12 km *param* model and we have found that this term dominates the differences. The average mass convergence measured around the inside of the shared inner domain shows increased convergence between 2–7 km in the 4 km *3Dsmag* model. There are also contributions from slightly higher surface evaporation rates and a reduction of total column water vapour in the 4 km *3Dsmag* run.

The models also exhibit a diurnal cycle that is too strong and too regular relative to TRMM (especially given that these are not local times but rather GMT). This is particularly true for the 12 km *param* model, which has an extremely regular diurnal cycle over the Maritime Continent land areas (Love *et al.*, 2011).

Domain-mean precipitation rates over only sea points (not shown) are overall similar to Figure 1, especially for TRMM, which shows very little difference. The 12 km *param* model is about 0.01 mm h^{-1} larger on average over sea, whereas the explicit convection models are approximately 0.01 mm h^{-1} smaller over sea points. The shape of the diurnal cycle is a more-regular sinusoid over sea points for all models and, to a lesser extent, for TRMM as well. The fact that the parametrized and explicit convection models become slightly closer to each other in terms of mean precipitation when land points are excluded agrees with the findings in Stephens *et al.* (2010).

4.2. Precipitation distributions

Figure 2(a) shows probability densities of precipitation rates (excluding zero values as described in section 2) averaged onto a 1° grid with 3 h temporal averaging. The precipitation rate has been aggregated into logarithmic-spaced histogram bins (with just over 26 bins per decade) and the probability density in each rain-rate bin is calculated as

$$P(r) = \frac{n(r)}{N\Delta r}, \tag{1}$$

where $P(r)$ is the probability density in the bin with mean rain rate r, $n(r)$ is the number of measurements in that bin, Δr is the bin width for that bin measured in mm h^{-1} and N is the total number of included measurements. Dividing by bin width is important because the bin width is not constant but rather increases in size logarithmically, so failure to normalize by bin width would result in a change in the slope of the plotted curve equivalent to adding -1 as compared with the same data plotted with equally spaced bins.

TRMM probability densities show roughly power-law behaviour at lower rain rates with an exponent of approximately -1, before decreasing more rapidly at higher values. Probability densities are much higher at high rain rates for the 4 km model runs and TRMM, while below about 1 mm h^{-1} the 12 km *param* model probability densities are much higher than those of the observations and other models. The fact that the 12 km *param* model has far too much light rain agrees with many earlier analyses of weather and climate models using convective parametrizations (Dai and Trenberth, 2004; Sun *et al.*, 2006; Wilcox and Donner, 2007; Stephens *et al.*, 2010).

The differences discussed above are even clearer when the probability densities are multiplied by bin-average precipitation rate and divided by domain-mean precipitation rate, yielding a fraction of total precipitation per rain rate contributed by each bin:

$$F(r) = \frac{rP(r)}{M} = \frac{r\,n(r)}{R\Delta r}, \tag{2}$$

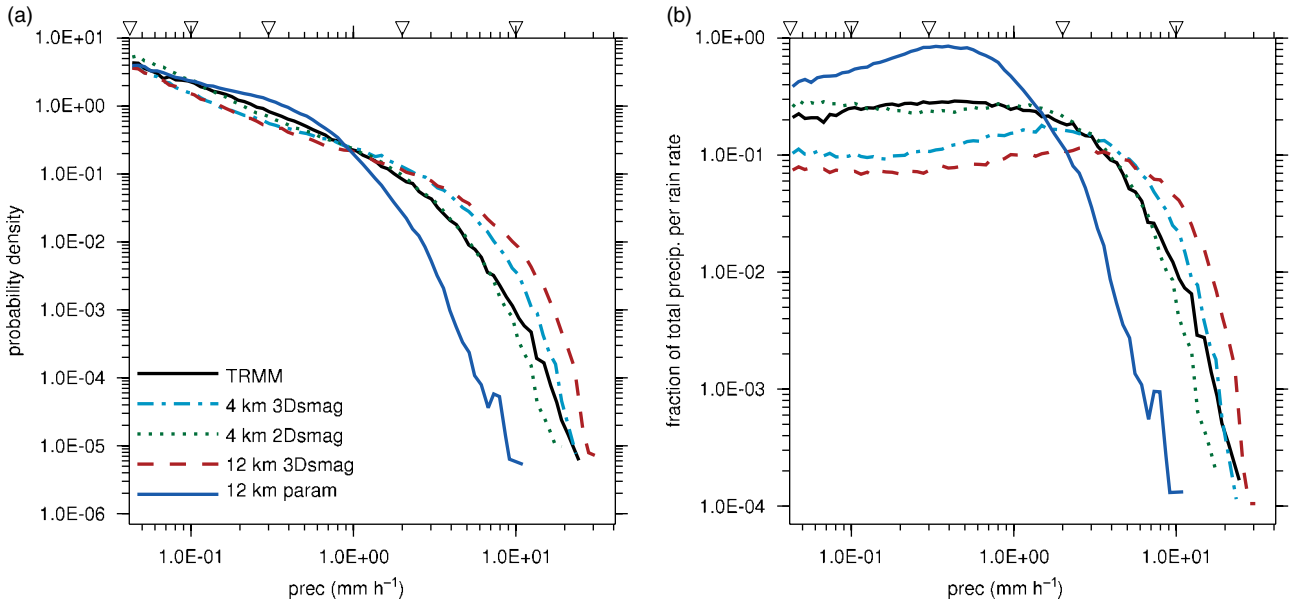

Figure 2. Precipitation distributions: (a) probability densities in $(\text{mm h}^{-1})^{-1}$, and (b) fractional rainfall amount densities in $(\text{mm h}^{-1})^{-1}$ for two 12 km Cascade runs, two 4 km Cascade runs and TRMM merged precipitation data over sea points, on a 1° latitude/longitude grid and 3 h time averages for 9 days starting on 7 April 2009. Triangles indicate specific rain rates discussed in the article.

where M is the mean rain rate for all included values (over sea, > 0.04167 mm h^{-1}) and R is the sum of all of these values, as shown in Figure 2(b). To aid interpretation of Figure 2, the values of $\{N,\ M\}$ for the 12 km *param*, 12 km *3Dsmag*, 4 km *2Dsmag*, 4 km *3Dsmag* and TRMM data are {186 616, 0.44}, {52 071, 2.11}, {120 102, 0.88}, {64 130, 1.56} and {73 281, 0.90}, respectively, with M in units of mm h^{-1}. The total number of possible values, including zero points, is 315 311 for each data source. These numbers are consistent with the discussion above regarding model differences, with more occurrences of rainfall at a fairly low average rain rate (near the apparent preferred scale) for the 12 km *param* model and fewer occurrences with higher average rain rates for the observations and the explicit convection models (with especially infrequent, heavy rain for the 4 km *3Dsmag* and 12 km *3Dsmag* models).

The rough power-law relationship of -1 for lower values of precipitation for both the 4 km runs and TRMM (Figure 2(a)) compares well with rain-rate distributions from several tropical observation sites (Peters *et al.*, 2010, their figure 1). This value of the power law implies an equal contribution at all scales, which is evident in Figure 2(b). In contrast, the 12 km *param* model curve has a pronounced bump around 0.4 mm h^{-1} (10 mm day^{-1}), implying a preferred rainfall rate (there are also less-pronounced peaks for the observations and the other model versions, particularly the 12 km *3Dsmag* and 4 km *3Dsmag* models, which could be slightly preferred rain rates as well). Precipitation distributions for a 40 km version of the model for the same case study and using parametrized convection (not shown) were very close to the 12 km *param* model distributions. This apparent preferred scale at low-to-moderate rain rates may be because the convective parametrization is constrained by the CAPE closure (with a 30 min relaxation time scale in this case) and a lack of mesoscale organization and its associated positive feedback between precipitation and local circulation/water vapour to produce steadier rainfall around the amount required by radiative cooling over the domain, given the convective area.

Compare Figure 2(b) with figure 4 of DeMott *et al.* (2007), which shows scale-free rain amounts for observations (GPCP) and the superparametrized Multi-scale Modeling Framework (MMF) but not for the regular Community Atmosphere Model (CAM) in the western Pacific, which has a bump around 10 mm day^{-1} similar to our 12 km *param* distribution. A possible explanation for similarity in the preferred rain rate for the CAM in the western Pacific in DeMott *et al.* (2007) and our 12 km *param* model is that the parametrized convection in both models is too tightly constrained to balance the large-scale forcing. Note that over the Amazon basin, however, even the MMF and observations have a bump around this precipitation rate.

A mechanism suggested by DeMott *et al.* (2007) to explain the CAM behaviour relates to the fact that the parametrized plumes in that model's convective parametrization (Zhang and McFarlane, 1995) must detrain above the level of minimum saturated moist static energy. Since the deep convection scheme must consume CAPE, the entrainment values for the plumes are forced to be very small in order for the plumes to maintain buoyancy while satisfying this constraint on the height of detrainment. Therefore, deep convection forms too quickly before shallow convection has had a chance to moisten lower levels, causing rain to occur too soon, too often and too lightly, and there is a corresponding lower- and mid-level dry bias. This mechanism could theoretically explain the behaviour of the 12 km *param* model, which also rains in relatively dry tropospheric air; however, our 4 km *2Dsmag* model has a large dry bias (see section 5.1) and still gets the rainfall distribution right, suggesting that there is perhaps something more universal that is allowed (or not forced to occur) in explicit convection, at least in the UM.

Note that the value of the preferred rain rate for the 12 km *param* model depends on horizontal averaging: when the model distributions are plotted using a 15 min averaging interval and the original 12 km *param* and 4 km grid size values, the 4 km *3Dsmag* model again shows no preferred scale across a large range, while the 12 km *param* model

has a peak that has shifted to values between about 2 and 4 mm h^{-1} (not shown). When the same 15 min data are plotted using 1° values (not shown), the plots look very similar to the 3 h average 1° grid, showing that this is a horizontal and not a temporal resolution dependence. A likely explanation for this is that, although on larger scales the average precipitation is constrained by radiative–convective equilibrium (and therefore agrees well with both M in the model and the preferred rain rate in the warm pool region in DeMott *et al.* (2007)), on smaller scales there is some mesoscale circulation feedback that allows some grid cells to rain at a consistently heavier rate at the expense of more-distant cells (typically, the heavier rain in the model occurs along lines of low-level convergence).

Field and Shutts (2009) found that instantaneous rain rates from UM operational forecasts with parametrized convection actually had too many instances of heavy rain relative to an idealized CSRM and satellite data. However, instantaneous rain rates from models will be sensitive to many parameters including model time step and, for parametrized convection, the number of times that the convection scheme is called as well as the relaxation time-scale for the closure; even instantaneous rain rates from observations imply a specific time scale. On the other hand, the 3 h accumulated rain-rate distributions from the parametrized convection model output in Field and Shutts (2009) have probability frequencies that are lower than or comparable to the CSRM instantaneous data at rain rates above 1 mm h^{-1} and higher at rain rates below this. Indeed, their dimensionless 3 h accumulated rain-rate distributions for the parametrized convection model output show a positive deviation from a power-law fit located at a rain rate of around 1 (the non-dimensionalized mean rain rate) similar to the findings in this article. To better compare our results with the plots in Field and Shutts (2009), we looked at the probability densities in Figure 2(a) using rescaled frequency ($P(r) \times M$) versus dimensionless rain rate (r/M), as in their study, and found that our results are not affected, with the 12 km *param* model still having higher frequencies than the observations and other model versions for non-dimensionalized rain rates between 0.3 and 1.2 and significantly lower frequencies above 1.4 (not shown).

4.3. *Sensitivity to subgrid-scale mixing*

As discussed above, one of the 4 km model versions (the 4 km *3Dsmag* model) uses 3-D Smagorinsky subgrid-scale mixing instead of using a traditional boundary-layer scheme for vertical mixing and only 2-D Smagorinsky (for horizontal mixing). This was motivated by results from smaller idealized convection runs showing that there is more-realistic moistening of the lower troposphere in 3-D Smagorinsky simulations. In the large-domain run, the 4 km *3Dsmag* version has larger areas of convective organization (including a much better MJO simulation) and larger areas of suppressed convection than the 4 km *2Dsmag* run (Holloway, Woolnough, and Lister, 2012; pers. comm.). In this respect, the 4 km *3Dsmag* run is closer to observations than the 4 km *2Dsmag* run. Also, the 4 km *3Dsmag* run has fewer areas of very isolated showers. Figure 2 shows that this also corresponds to 4 km *3Dsmag* precipitation distributions, which are somewhat too low at very low precipitation rates and slightly too high at higher rates relative to TRMM data. However, this might be expected for explicit convection with a grid size greater than 200 m or so, since large amounts of instability must build up until the entire grid cell begins to undergo convection, at which point rain rates can be quite strong; Khairoutdinov *et al.* (2009) found that small-scale water vapour and cloud properties did not approach convergence until at or below 200 m grid spacing for explicit convection simulations of tropical maritime convection ranging from 100–1600 m, although there were very similar equilibrium large-scale rain rates. Indeed, the 12 km *3Dsmag* explicit convection run, also using 3-D Smagorinsky mixing, has a precipitation distribution shifted even further toward higher values. Zhou *et al.* (2007) also found that CSRM simulations over the South China Sea produced greater fractions of their rainfall from high rain rates than did satellite observations.

5. Vertical structure by precipitation rate

The tendency to have a preferred scale of rainfall rate and, relatedly, to have too much light rain and too little heavy rain compared with observations seems to be a consequence of parametrized convection over the Indo-Pacific warm pool. In this section, we analyze the vertical structure of the different model runs and analyses to compare different convective regimes and the processes operating within them. The goal is to suggest possible mechanisms generating the differences in precipitation distributions as well as the consequences for larger scale waves and dynamics of different distributions of precipitation and associated heating, moistening and circulation patterns.

5.1. *Environmental conditions by rain rate*

Many studies have found a strong relationship between tropospheric water vapour and precipitation in observations (Bretherton *et al.*, 2004; Peters and Neelin, 2006; Holloway and Neelin, 2009) and CSRMs (Grabowski, 2003; Derbyshire *et al.*, 2004; Bretherton *et al.*, 2005). However, parametrized convection usually lacks this strong relationship; in particular, models with parametrized convection tend to have too much light rain falling in relatively dry tropospheric conditions (Thayer-Calder and Randall, 2009, their figure 4). The sensitivity of convection to free-tropospheric moisture has been shown to depend largely on entrainment within convective parametrizations and simple plume models, with larger entrainment rates yielding a greater, more-realistic sensitivity to moisture by helping to suppress deep convection in regions with drier free-tropospheric air (Derbyshire *et al.*, 2004; Holloway and Neelin, 2009).

To investigate the distribution of subsaturation (the relevant quantity to assess the impact of entrainment drying on convective plumes), Figure 3 shows the saturation deficit, defined as $q_s - q$, where q is the specific humidity and q_s is the saturation specific humidity, for the different model runs and ECMWF analyses at different precipitation rates. (Note that we use TRMM precipitation for the ECMWF panel, not the precipitation in the analyses themselves, since the satellite observations should be closer to truth than the operational analyses; ECMWF column water vapour agrees well with TMI column water vapour, as discussed above in section 2, and Holloway and Neelin (2009) showed that column water vapour is highly correlated with lower-free-tropospheric moisture in tropical radiosonde data). Standard-error values are nearly all below 0.1 g kg^{-1}, with

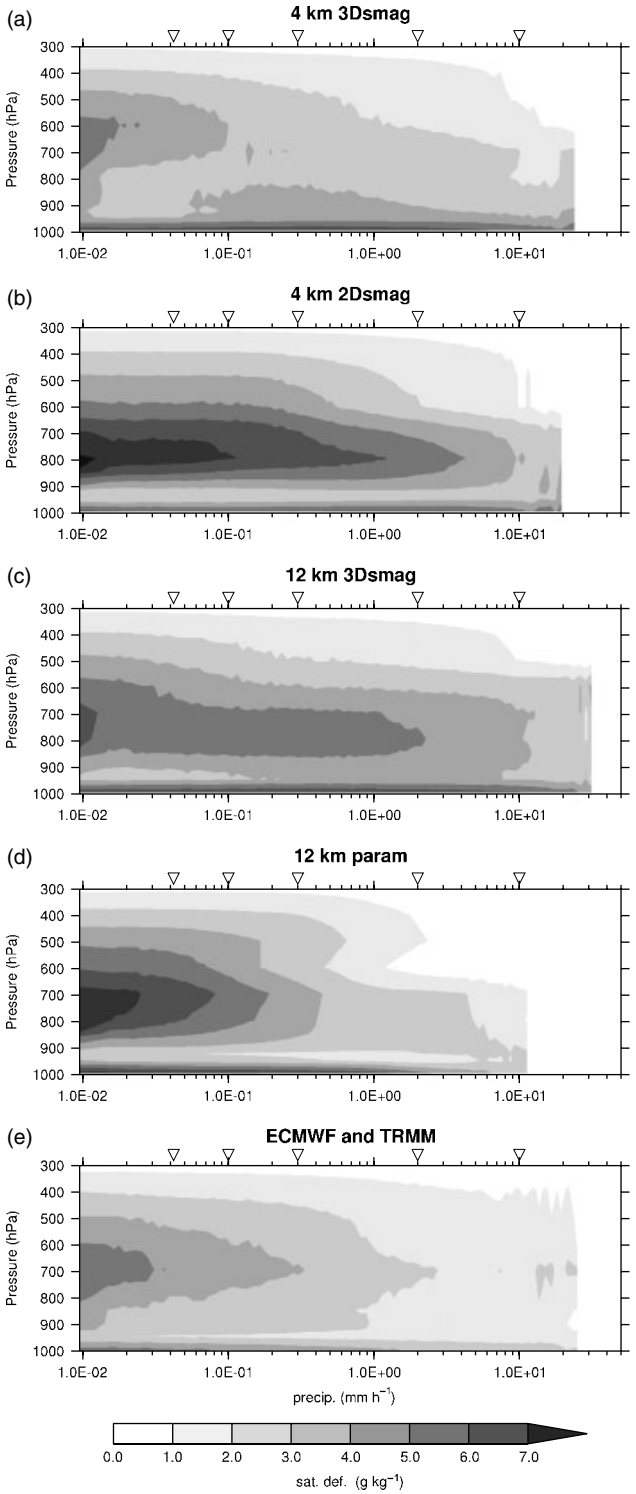

Figure 3. Saturation deficit composited on precipitation rate using 1° 3-h averages over sea for (a) 4 km *3Dsmag*, (b) 4 km *2Dsmag*, (c) 12 km *3Dsmag*, (d) 12 km *param* and (e) ECMWF analyses (conditioned on TRMM precipitation) for 9 days starting on 7 April 2009. Triangles indicate specific rain rates discussed in the article.

a few values reaching 0.6 in the highest precipitation bins because of the limited sample numbers. The 4 km *3Dsmag* run shows significant subsaturation at mid-levels for light rain rates (below 1.0 E−1 mm h^{-1}) but much lower values at moderate and high rain rates, which is overall very similar to the ECMWF analyses. In contrast, the 12 km *param* run shows much drier free-tropospheric air at low and moderate rain rates (below 3.0 E−1 mm h^{-1}). On the other hand, the 4 km *2Dsmag* run shows even drier lower-free-tropospheric air for nearly all precipitation rates. The 12 km *3Dsmag* explicit convection run also shows a fairly dry lower free troposphere, although it has a fairly small gradient of saturation deficit with increasing precipitation rate at these levels, which agrees more with ECMWF.

Since the 4 km *2Dsmag* run still produces a precipitation distribution similar to observations, it seems unlikely that the sensitivity of convection to free-tropospheric moisture is the main process lacking in the 12 km *param* convection that would be needed to reproduce a realistic precipitation distribution. However, it is a likely candidate for other problems, shown in both the 12 km *param* and 4 km *2Dsmag* runs but not the 4 km *3Dsmag* run, in large-scale organization, including MJO propagation (Holloway, Woolnough, and Lister, 2012; pers. comm.). These composites of subsaturation are also important in understanding the implications of the different precipitation distributions for large-scale waves and circulations (discussed in section 6 below). One feature of Figure 3 is that the 12 km *param* model is even closer to saturation than ECMWF and all of the other models for rain rates greater than 2.0 E+0 mm h^{-1} and vertical levels in range 600–400 hPa; this unique behaviour in the parametrized convection run at high rain rates is discussed further below as an indicator of a possible mechanism for its lack of heavy rain.

Moist static energy (h) and saturation moist static energy (h_s) profiles are shown in Figure 4, with corresponding profiles of saturation deficit and relative humidity shown in Figure 5, for the overall mean and five selected rain rates for the 12 km *param*, 4 km *3Dsmag* and 4 km *2Dsmag* models. Standard-error values are all below 0.2 kJ kg^{-1} for Figure 4 and below 0.1 g kg^{-1} and 1% for Figure 5, with values approaching 1 kJ kg^{-1}, 0.5 g kg^{-1} and 7%, respectively, at 1.0 E+1. Note that we exclude the 12 km *3Dsmag* model from further analysis for visual clarity and because that model was primarily run as confirmation of our hypothesis that explicit versus parametrized convection made a much bigger difference in behaviour than horizontal resolution.

Since h_s depends only on temperature and pressure, the h and h_s curves together can be used to estimate the undiluted CAPE and convective inhibition for parcels lifted from various levels in the boundary layer. A lifted parcel will approximately conserve h, and once it has reached saturation its buoyancy is proportional to its difference from the h_s curve; undiluted CAPE is proportional to the positive area between this curve and a straight vertical line drawn from a boundary-layer h value. However, this does not include the effects of entrainment mixing, which are likely to be very important where there are large saturation deficits.

Comparing the mean values for the three model versions, there is a significantly lower amount of h through much of the troposphere for the 4 km *3Dsmag* model and 4 km *2Dsmag* model, consistent with much drier air in the case of the 4 km *2Dsmag* model and cooler, slightly drier air in the case of the 4 km *3Dsmag* model (see Figure 5). This lower mean h may simply reflect the larger number of grid points with rain rates below 4.2 E−2 mm h^{-1} for the 4 km model runs, suggesting that these models are more able to produce suppressed convective regions. At upper-tropospheric levels, h_s shows a slightly less-stable (more-vertical) profile for the 12 km *param* model. There is also a much shorter vertical

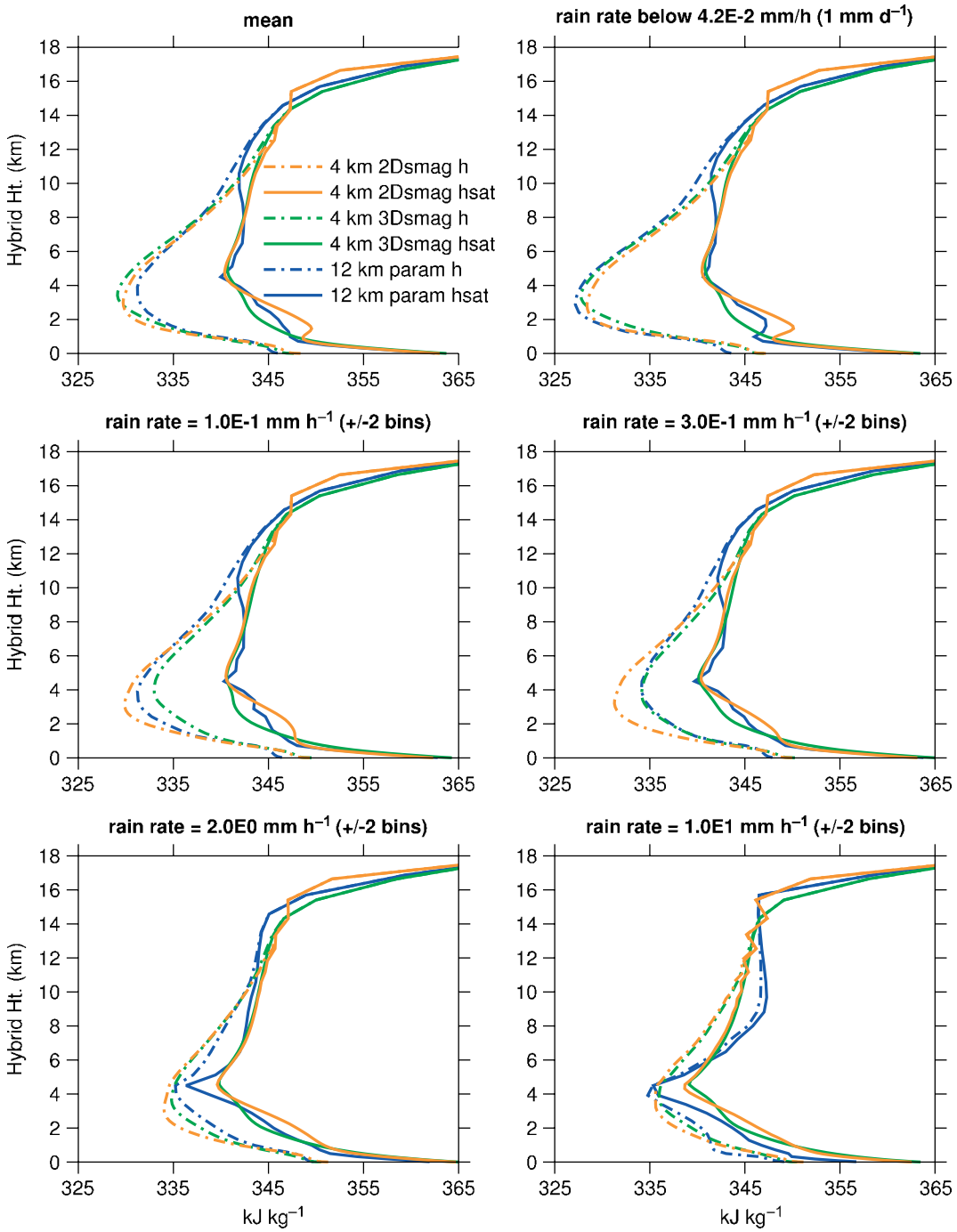

Figure 4. Moist static energy (dash–dotted lines) and saturated moist static energy (solid lines) composites for the mean and five rainfall bins using 1° 3 h averages over sea for 9 days starting on 6 April 2009.

distance before lifted undiluted near-surface parcels become buoyant for the 4 km *3Dsmag* model (∼1 km compared with ≥2 km for the other models), possibly indicating more-realistic shallow convection. In addition, there is a sharper kink near the freezing level for the 12 km *param* model h_s.

While mean relative humidity and saturation deficit are very similar for the 12 km *param* model and the 4 km *3Dsmag* model, for the 4 km *3Dsmag* model this deficit is steadily reduced with increasing rainfall, starting at lower levels and gradually being reduced more and more at upper levels (Figure 5). The 12 km *param* model has much larger saturation deficits than the 4 km *3Dsmag* model at light rain rates (1.0 E−1 mm h^{-1} and below) and even slightly larger saturation deficits at moderate rates (3.0 E−1 mm h^{-1}), although this model is extremely close to saturation at higher rain rates compared with the other models. The 4 km *2Dsmag* version is even dryer than the 12 km *param* model in the boundary layer and lower troposphere at nearly all rain rates, consistent with the saturation deficit composite contours in Figure 3. This is likely due to insufficient mixing of the boundary-layer scheme for this version of the model. However, in the middle and upper troposphere at the two highest rain rates, both of the 4 km model versions are significantly drier than the 12 km *param* model.

While the 4 km *2Dsmag* model is unable adequately to simulate large-scale variability such as the MJO, as mentioned above, it is instructive to compare thermodynamic

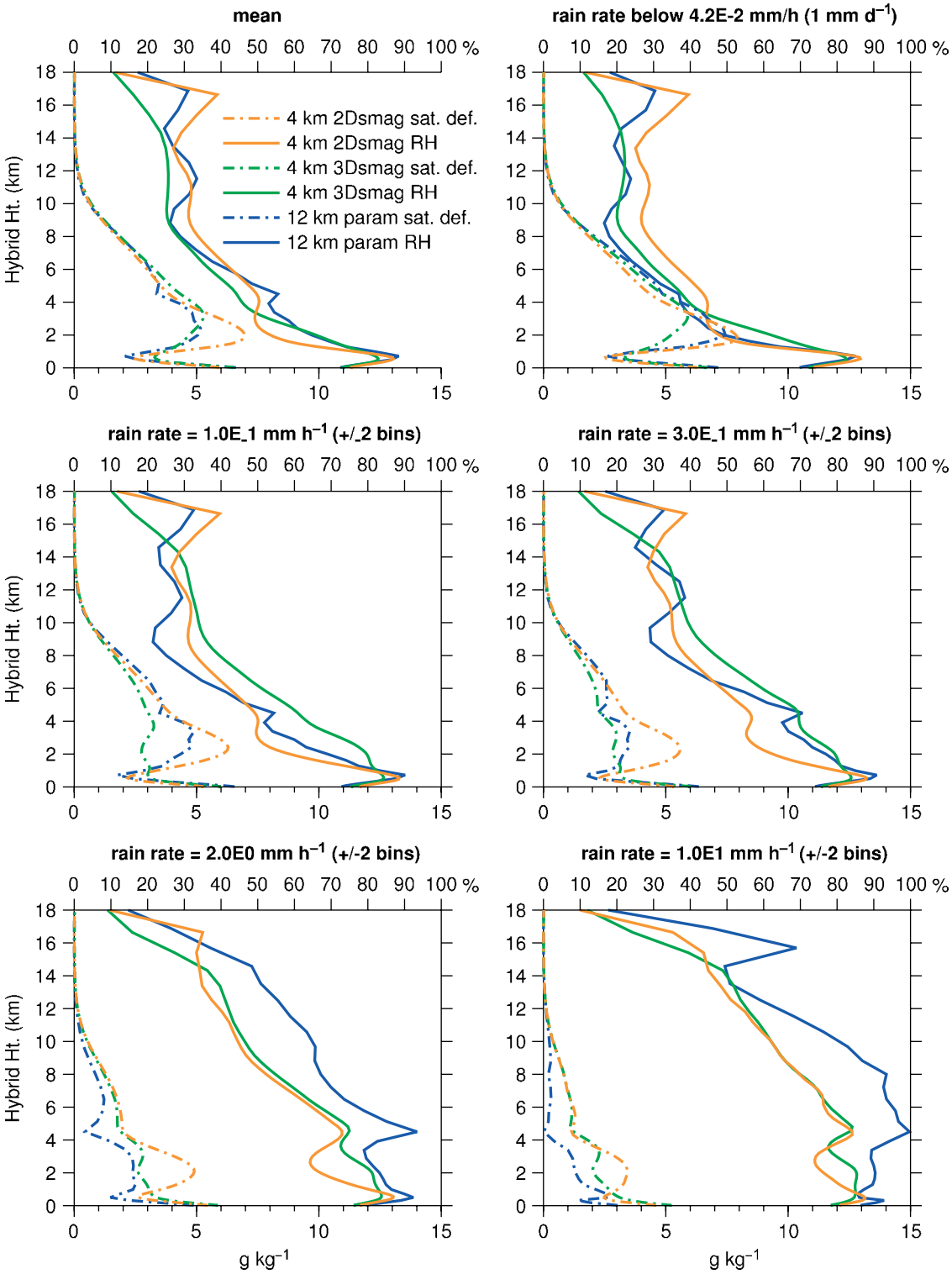

Figure 5. Saturation deficit (dash–dotted lines, lower axes) and relative humidity (solid lines, upper axes) composites for the mean and five rainfall bins using 1° 3 h averages over sea for 9 days starting on 6 April 2009.

profiles of this model with those of the 12 km *param* and 4 km *3Dsmag* models to make inferences about why the explicit convection runs (the two 4 km runs in this case) are better able to simulate the observed precipitation distribution. For instance, there is a much more consistent temperature structure in the upper troposphere in the 4 km models across the different rain rates, with h_s increasing somewhat linearly with height. In contrast, the 12 km *param* model has a more vertical h_s profile in the upper troposphere, which becomes much warmer at high precipitation rates. One possibility is that heavy rainfall in the 12 km *param* model is only possible for very moist lower-tropospheric conditions where the entire region is fairly close to saturation, leading to less drying of convective plumes via entrainment and therefore warmer moist adiabats and increased convective heating which could then quickly stabilize the profile and reduce the likelihood of more heavy rain in that region.

Composites of vertical velocity on precipitation rate are shown in Figure 6 for four model versions (we do not include ECMWF operational analyses because their vertical

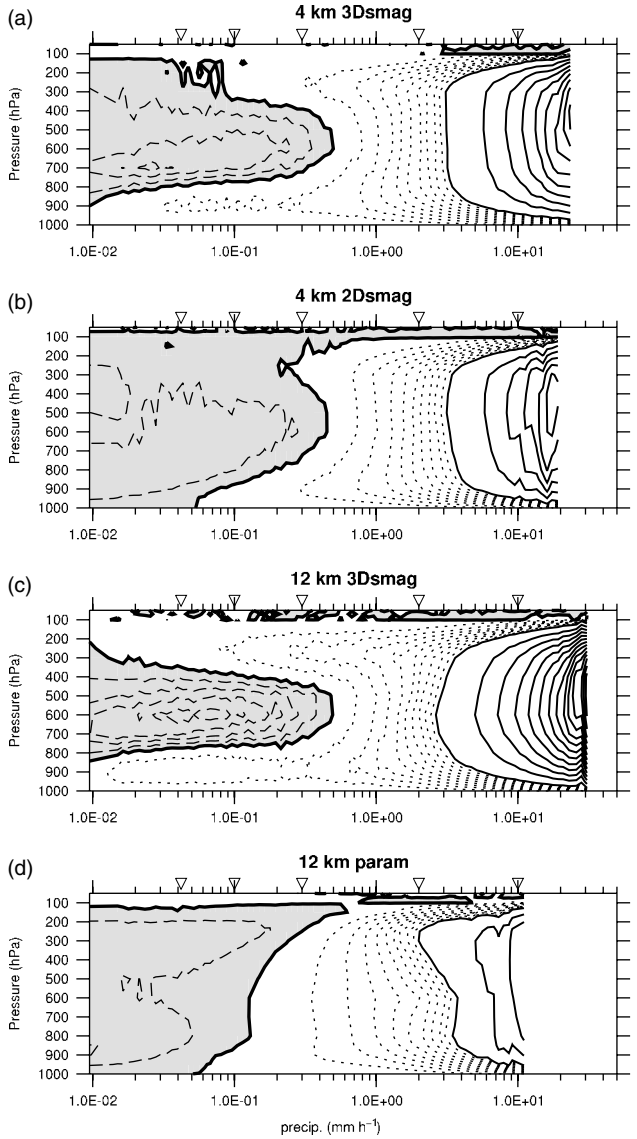

Figure 6. Pressure velocity composited on precipitation rate using 1° 3 h averages over sea for (a) 4 km *3Dsmag*, (b) 4 km *2Dsmag*, (c) 12 km *3Dsmag* and (d) 12 km *param*, for 9 days starting on 7 April 2009. Contour intervals are 0.5 Pa s^{-1} (solid lines), 0.05 Pa s^{-1} (dotted lines) and 0.025 Pa s^{-1} (dashed lines), all starting from the zero contour (thick solid line), with positive region (downward motion) shaded. Triangles indicate specific rain rates discussed in the article.

velocity fields are likely to be more representative of the forecast model physics than the assimilated data). Standard-error values are all below 0.01 Pa s^{-1} for precipitation-rate bins below 2.0 E+0, with a few values reaching 0.7 for the highest precipitation bins. These velocities are the average on the 1° grid of the resolved vertical velocities. Parametrized convection yields no net vertical velocity on the resolved original grid scale, since convective updraughts are exactly balanced by downdraughts and subsidence. Explicit convection has no such imposed balance at any scale (other than mass continuity). Averaging on to the 1° grid should yield small net vertical motion associated with resolved convective motion (including compensating subsidence) in the explicit convection runs (particularly for the 4 km explicit convection runs, which have many more grid boxes in each 1° grid box). This is equivalent to the scale-separation assumption in convective parametrizations. Any differences between the 1° average vertical velocities of the parametrized convection and explicit convection models reflect weaknesses in that assumption or the effect of differently simulated convective processes on the large-scale circulation, not the averaging technique used.

The 4 km *3Dsmag* model and the 12 km *3Dsmag* model are the only model versions to have upward velocity (at least at low levels) at all precipitation rates, suggesting explicit shallow convection at low rain rates. In fact, the 4 km *3Dsmag* model and the 12 km *3Dsmag* model both have percentages of rainfall contributed by the convective parametrization that range from less than 1% at and above rain rates of 1.0 E−1 mm h^{-1} to 5% and 3%, respectively, at 1.0 E−2 mm h^{-1}. In contrast, the 4 km *2DSmag* model, while still having less than 1% of all rainfall contributed by the convective parametrization, has about 4% of its rainfall at 1.0 E−1 mm h^{-1} contributed by convective parametrization and this increases to 36% as the rain rate goes down to 1.0 E−2 mm h^{-1}, showing that much of the rain at very low rain rates is coming from the parametrization. The 12 km *param* model has over 99% of its rainfall contributed by the convective parametrization at all rainfall rates below 3.0 E+0 mm h^{-1}, with this percentage dropping to as low as 86% within the range of highest model rain rates. The differences in the amount of parametrized convection at very low rain rates might also explain why there is relatively less light rain for the 4 km *3Dsmag* and 12 km *3Dsmag* models.

The 12 km *param* model tends to have relatively top-heavy upward velocity profiles for high precipitation values and subsidence at all levels for very low rain rates. For very heavy rainfall, the 12 km *param* model is more top-heavy than any of the explicit convection runs; we know from Figure 4 that it is warmer in the 12 km *param* run in the upper troposphere than for either of the 4 km runs for the highest rain rate, again suggesting that it may be very difficult to maintain heavy rain for long because of very strong stabilization effects. The different precipitation distribution in the 12 km *param* model relative to the other model runs (Figure 2) means that the overall pattern of resolved free-tropospheric vertical velocity in rainy regions will be much weaker than for the explicit convection runs, which will have implications for large-scale waves and circulation (see discussion in section 6 below). Another difference between the 12 km *param* model and the other model runs is that the 12 km *param* model has upward motion through most of the troposphere for rain rates greater than 2.0 E−1 mm h^{-1}, including within the range of its preferred rain rate, whereas the other models have mid-tropospheric subsidence for rain rates below about 4.0 E−1 mm h^{-1}.

5.2. *Heating and moistening rates by rain rate*

The temperature and moisture budgets for a given large-scale region can be illustrated by writing the total tendency and large-scale advection terms equal to the apparent heat source Q_1, radiative heating Q_R and apparent moisture sink Q_2 (Yanai *et al.*, 1973; Ciesielski *et al.*, 1999) as follows:

$$\Pi\left(\frac{\partial\bar{\theta}}{\partial t}+\nabla\cdot(\bar{\mathbf{v}}\bar{\theta})+\frac{1}{\bar{\rho}}\frac{\partial(\bar{\rho}\bar{w}\bar{\theta})}{\partial z}\right)=\frac{1}{c_p}(Q_1+Q_R), \quad (3)$$

$$\frac{\partial\bar{q}}{\partial t}+\nabla\cdot(\bar{\mathbf{v}}\bar{q})+\frac{1}{\bar{\rho}}\frac{\partial(\bar{\rho}\bar{w}\bar{q})}{\partial z} = -\frac{1}{L}Q_2, \quad (4)$$

where θ is potential temperature, q is specific humidity, $\mathbf{v}$ is the vector horizontal velocity, w is the vertical velocity, c_p

is the specific heat of dry air at constant pressure, L is the latent heat of condensation, ρ is the density, Π is the Exner function defined as

$$\Pi = \left(\frac{\bar{p}}{p_0}\right)^{R/c_p},$$

R is the gas constant for dry air, p is the pressure and $p_0 = 1000$ hPa is the reference pressure. $\{\bar{}\}$ denotes the horizontal average at a single level and time over the 'large scale' (1° in this case). Although these equations are often used to describe the separation between resolved and parametrized processes, they can equally be used for any area average to distinguish between net advective fluxes into the area and net advective (vertical transport) fluxes, turbulent fluxes and physical processes occurring within the area. Here we apply this budget analysis to the 1° grid boxes. We will therefore use the terms 'large-scale' and 'subgrid' with this in mind, as described below. Note that we have defined Q_R as a separate term rather than including it as part of Q_1, unlike Yanai *et al.* (1973) and some other articles. Q_1 and Q_2 can then be related to net condensation and vertical subgrid transport as

$$\frac{1}{c_p} Q_1 = \frac{L}{c_p}(c - e) - \frac{\Pi}{\bar{\rho}} \frac{\partial \overline{\rho w' \theta'}}{\partial z}, \quad (5)$$

$$-\frac{1}{L} Q_2 = -(c - e) - \frac{1}{\bar{\rho}} \frac{\partial \overline{\rho w' q'}}{\partial z}, \quad (6)$$

where c is condensation and e is evaporation of condensate; only liquid–vapour phase transitions are included in the equations for simplicity, although in the model calculations ice-phase transitions are also accounted for. $\{'\}$ denotes the anomaly from the horizontal average, $\{\bar{}\}$, defined above.

Figures 7 and 8 show the total, subgrid-scale and large-scale heating and moistening averaged for all points below 4.2 E−2 mm h^{-1} and for three higher rain rates for the 12 km *param* and 4 km *3Dsmag* runs. The total tendencies are represented by the first term in (3) and (4), with the large-scale advection represented by the second and third terms. The subgrid-scale terms (and radiation term for temperature) are shown on the right-hand side of (3) and (4), with the subgrid terms further defined by (5) and (6). Standard-error values are all below 0.5 K day^{-1} for Figure 7 and 0.3 g kg^{-1} day^{-1} for Figure 8.

The subgrid terms in Figures 7 and 8, given by (5) and (6), are calculated by first adding the increments to temperature and moisture from the convective parametrization, boundary-layer/large-scale cloud scheme (including vertical subgrid turbulence mixing and surface temperature and moisture fluxes), large-scale rain scheme and horizontal subgrid turbulence mixing (which is very small and is not used for the 12 km *param* model). Note that 'large-scale' in 'large-scale rain' and 'large-scale cloud' refers to the original model grid scale and these schemes are considered 'subgrid' processes here. Additionally, the last term in (5) and (6), the vertical transport of heat and moisture from subgrid-scale motions, while partly included in the convective, mixing and surface-flux terms already accounted for in the model increments listed above, will also be partly represented by explicit vertical advection at each model's own grid scale. This is particularly true for the explicit convection runs. To account for this, we estimate these explicit subgrid fluxes from instantaneous anomalies every hour within each 1° large-scale grid box and then terms are averaged over three-hourly periods and added to the other subgrid terms listed above.

The large-scale advection terms are calculated by using the temperature and moisture increments from the advection scheme and then subtracting the explicit subgrid vertical transport term, calculated as described above. The radiation and total tendency terms come directly from model increments, with any small residuals in the budget added to the subgrid term so that the budget is balanced. All terms are averaged onto the 1° grid scale and three-hourly temporal scale.

For heating, the subgrid term for the 4 km *3Dsmag* model is mainly made up of a combination of the large-scale rain scheme and the boundary-layer/large-scale cloud scheme, while for moisture the transport term is also important. The 12 km *param* subgrid heating and moistening is dominated by the convection scheme at all rain rates except in the boundary layer, where the boundary-layer/large-scale cloud scheme is also important.

In most cases, the subgrid terms nearly balance the large-scale advection, although radiation is sometimes important in the heating budget, particularly at lighter rain rates (also note that the subgrid and large-scale advection terms are plotted on a larger scale at high precipitation rates). At very low rain rates (below 4.2 E−2 mm h^{-1} or 1 mm day^{-1}, where deep convection is likely suppressed), the two models are mostly in agreement, although there is slightly more warming and drying above the boundary layer for the 12 km *param* model in the total field increments. At light to moderate rain rates (1.0 E−1 and 3.0 E−1 mm h^{-1}) the total increments show that the 4 km *3Dsmag* run has significant drying and warming in the boundary layer (below 2 km) that is not seen in the 12 km *param* model, as well as more warming and slightly more moistening in the lower free troposphere. This is associated with subgrid increments with significantly more moistening in the free troposphere and drying in the boundary layer as well as mid-tropospheric cooling; these are likely related to more shallow convection and/or evaporation of stratiform rainfall (although the relationship between subgrid terms and total increments can be complicated to explain). The subgrid moistening profiles at rain rates of 1.0 E−1 mm h^{-1} and 3.0 E−1 mm h^{-1} for the 4 km *3Dsmag* run are similar to the suppressed period CSRM integrations in (Woolnough *et al.*, 2010, their figure 8), although the magnitude in the 12 km *param* model is more similar to those profiles at 1.0 E−1 mm h^{-1}; the precipitation in the CSRMs compared in the suppressed period of that study ranges from 4.0 E−2 to 1.0 E−1 mm h^{-1}. Interestingly, the lowest rain-rate bin in our Figure 8, with rain rates lower than those in the suppressed period CSRMs in Woolnough *et al.* (2010), shows strong moistening at levels below 2 km for both model versions, somewhat lower than shown by the CSRMs (at somewhat higher rain rates) in that study.

At large precipitation rates (2.0 E+0 mm h^{-1}), both models show strong subgrid drying and warming throughout the troposphere, but the total increment for moisture shows significant low-level drying below 2 km and free-tropospheric moistening above 4 km in the 4 km *3Dsmag* run, which is almost absent in the 12 km *param* run. The subgrid heating in the 12 km *param* model is stronger at upper-tropospheric levels (6–12 km) at the highest rain rate than in the 4 km *3Dsmag* model, agreeing with the discussion in section 5.1

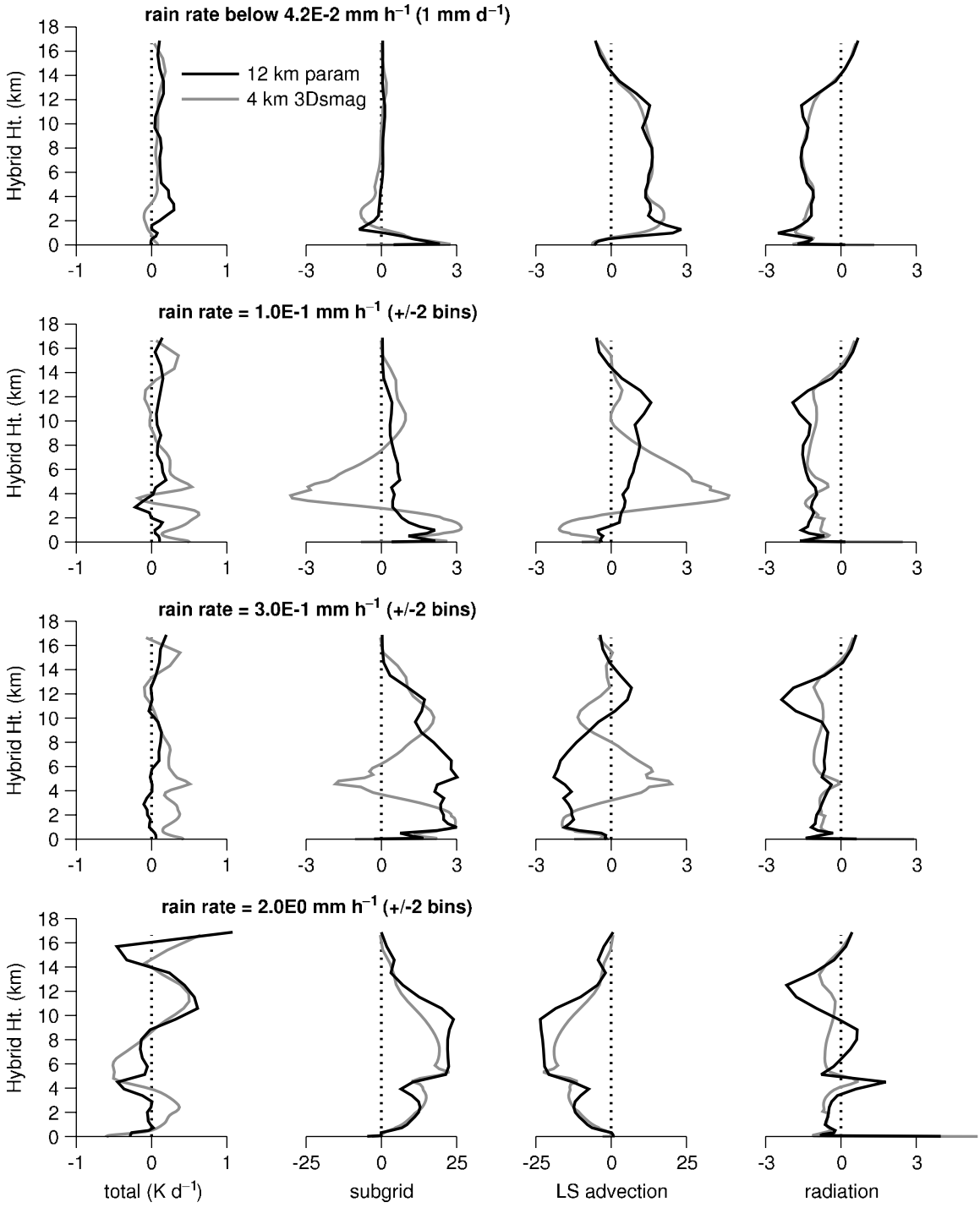

Figure 7. Average total temperature tendency and its three component terms (subgrid processes, large-scale advection and radiation) for four rainfall bins using 1° 3 h averages over sea for 9 days starting on 6 April 2009.

suggesting that more upper-tropospheric stabilization for heavy rainfall in the 12 km *param* model might be a cause of it being very difficult for that model to produce very heavy rain.

Note that there are obvious large differences in the vertically integrated drying and heating (which would be found by vertically integrating subgrid terms suitably weighted by density and multiplying by appropriate constants) for the two models, even at the same precipitation rate. Since the subgrid terms represent the effects of surface evaporation as well as conversion between liquid or solid condensate and water vapour, these are partly due to differences in surface evaporation rates and partly due to the advection of condensate and changes in the total condensate for a given rain rate: for instance, at 3.0 E−1 mm h^{-1} the 4 km *3Dsmag* model has about 1.0 E−1 mm h^{-1} (one third) of the rain rate explained not by subgrid moisture tendencies but by the advection of liquid and ice condensate into the 1° box (7.0 E−2 mm h^{-1}) and also a reduction in the condensate reservoir of the box (3.0 E−2 mm h^{-1}), whereas these two terms are negligible in the 12 km *param* model. The mid-tropospheric cooling and moistening in the subgrid terms show the effects of evaporation of these falling hydrometeors.

The subgrid heating profiles at the highest rain rates are more top-heavy than some of the Tropical Ocean

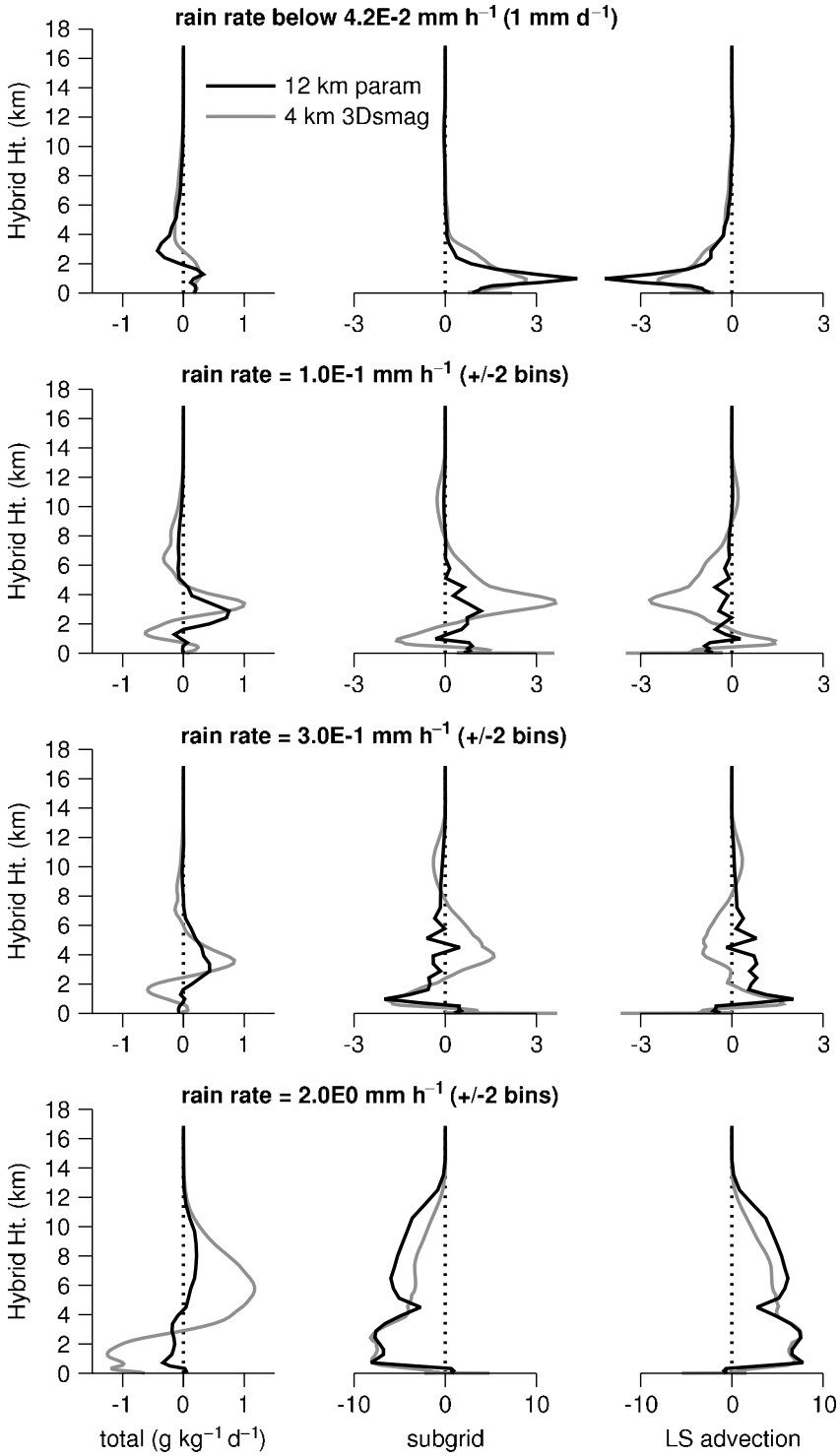

Figure 8. Average total moisture tendency and its two component terms (subgrid processes and large-scale advection) for four rainfall bins using 1° 3 h averages over sea for 9 days starting on 6 April 2009.

Global Atmosphere Program's Coupled Ocean Atmosphere Response Experiment (TOGA-COARE) estimates and Goddard Cumulus Ensemble (GCE) CSRM estimates in Shige *et al.* (2007), although their shapes are similar to TRMM estimates of latent heating in that study over various tropical convective regions. The top-heaviness of the heating profiles agrees with the overall conclusion of Lin *et al.* (2004) that MJO active events have more upper-tropospheric heating, relative to total heating, than mean tropical rainfall. However, it is difficult to compare these profiles directly with most other studies, since these are averages not over regions but rather over rainfall regimes, which occur over many locations and times.

For the *subgrid* heating and moistening terms, the models agree fairly well at the highest precipitation rate but are very different at the lower rain rate of 1.0 E−1 mm h^{-1}. The 4 km *3Dsmag* model exhibits cooling and moistening at mid-levels and warming and drying at low levels, while the 12 km *param* model shows much less, with perhaps slight warming and moistening at low levels for subgrid terms. Looking only at what convection does directly (the subgrid terms), the 4 km *3Dsmag* model would seem to take longer in the transition

to deeper convection, while the 12 km *param* model might transition to deep convection more quickly (especially given its tendency to rain at profiles with dryer mid-levels anyway, likely due to small entrainment rates) and therefore might consume CAPE more quickly and not maintain extended heavy precipitation because the CAPE never builds up, similar to arguments from DeMott *et al.* (2007). However, it is not as simple as arguing that rainfall occurs only in moister tropospheric conditions, since the 4 km *2Dsmag* model still gets the rainfall distribution right. There may be other reasons why CAPE is able to build up for longer locally before heavy rain begins. However, there may also be reasons why rainfall in the 4 km models is able to release potential energy from larger regions via circulation feedback, which does not operate to the same degree in the 12 km *param* model.

6. Discussion

The different heating and moistening profiles in the 12 km *param* and 4 km *3Dsmag* model runs, as well as the differences in environmental conditions, have important implications for larger scales. This is true both because of the differences at any given rain rate and because of the differences in the rainfall distributions, meaning that the 12 km *param* model will have more regions dominated by conditions and increments typical of its preferred, fairly light, rain rate (represented in Figures 7 and 8 by the composites around 3.0 E−1 mm h^{-1}). In the first instance, the discussion in section 5.2 above points out differences at the lightest rain rates (in relatively suppressed conditions) that would tend to cause more mid-level moistening and destabilization of the column in the 4 km *3Dsmag* run relative to the 12 km *param* run, allowing for a transition to less convectively suppressed conditions.

The second consideration above stems from the fact that the 12 km *param* model has far less heavy rain than the 4 km *3Dsmag* run. Even though both models have at least some drying throughout most of the lower troposphere at high rain rates, the 12 km *param* model has relatively few regions with these tendencies. As a result, it is likely more difficult for active convective regions to become drier and transition to more suppressed regions as they do in the MJO. Indeed, an upcoming paper (Holloway, Woolnough, and Lister, 2012; pers. comm.) will discuss the fact that the 12 km *param* model tends to maintain a single phase of the MJO rather than allowing it to propagate eastward.

The tendency for slow moistening at fairly light rain rates, drying at heavier rain rates and fairly small tendencies in between, is one possible mechanism to explain the preferred scale for the 12 km *param* model. However, this would be a stronger case to make for a model with a good sensitivity of convection to free-tropospheric moisture, which does not appear to be present in the 12 km *param* model based on Figure 3.

At the same time, in section 5.1 and section 5.2 it is argued that at high rain rates more heating at upper levels in the 12 km *param* model may lead to increased stabilization and a quick termination of any very heavy rainfall (although greater lower-level drying in the 4 km *3Dsmag* model could do the same thing). The 12 km *param* model also has a much weaker pattern of resolved vertical velocity associated with nearly all rain rates (Figure 6): there is much less upward motion at higher rain rates than for any of the other models and less subsidence at very low rain rates than for the 4 km *3Dsmag* or 12 km *3Dsmag* models. This will be skewed even further toward areas of low vertical motion by the fact that the 12 km *param* model has a rainfall distribution more tightly distributed around low-to-moderate rain rates. At large rain rates, the 12 km *param* model has a more-top-heavy upward vertical velocity pattern as well, which agrees with relatively strong heating at upper-tropospheric levels. Taken together, these patterns suggest that the 12 km *param* model has a weaker overturning circulation between active and suppressed convective regions than the other models, with an added possibility that stabilization occurs more quickly at very high rain rates.

Although not shown, the increments for temperature and moisture in the 4 km *2Dsmag* run at higher rain rates are broadly similar to those of the 4 km *3Dsmag* run: much more lower-level drying and mid- to upper-level moistening in the total moisture increment and less-top-heavy warming in the subgrid temperature increment. Since we know that the 4 km *2Dsmag* run has a very poor sensitivity of precipitation to moisture (Figure 3) and yet still produces a very realistic precipitation distribution (Figure 2), this is again a hint that these differences may be important for simulating precipitation distributions.

To show how the combination of differences in moistening rates at a given precipitation rate and differences in precipitation distributions gives important overall differences in moistening for the two models, Figure 9 shows the total moisture tendency for rainfall rates below 4.2 E−2 mm h^{-1} and the three terciles between this value and the maximum precipitation rate. Standard-error values are all below 0.05 g kg^{-1} day^{-1}. The figure shows that the 4 km *3Dsmag* model has significantly more low-level drying at all three

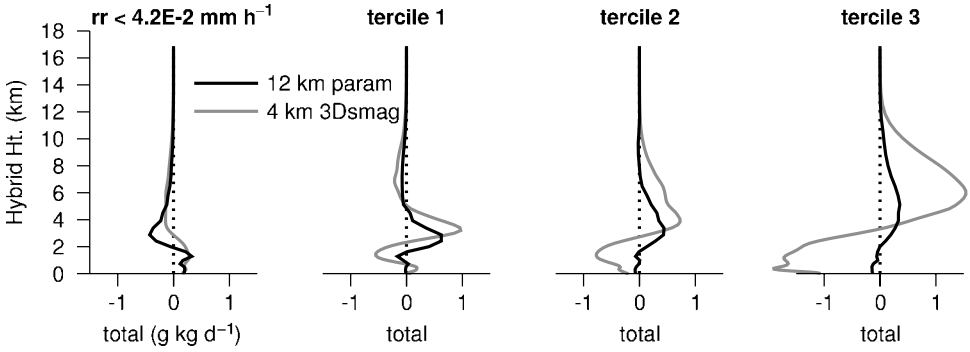

Figure 9. Average total moisture tendency for rainfall rates below 4.2 E−2 mm h^{-1} and the three terciles between this value and the maximum precipitation rate for two model versions using 1° 3 h averages over sea for 9 days starting on 6 April 2009.

rainy terciles than the 12 km *param* model, which must do virtually all of its drying in the suppressed regions. There is also more moistening in the upper terciles for the 4 km *3Dsmag* model and it is relatively higher in altitude. Note that there are many more rainy values in the 12 km *param* model: 19.7% of the total values are in each tercile, with 40.9% in the suppressed, low-precipitation bin. For the 4 km *3Dsmag* bin, these numbers are 6.8% and 79.6%, respectively. The mean moistening rate over all values, which is obtained by taking a weighted average of the four curves in Figure 9 using the population percentages given above as weights for each model, is small: about 0.07 g kg^{-1} day^{-1} in the lower free troposphere in the 12 km *param* model and 0.02 g kg^{-1} day^{-1} in the troposphere for the 4 km *3Dsmag* model. The upper limits of the three terciles for the 12 km *param* and 4 km *3Dsmag* models are {0.18, 0.46, 11.04} and {0.34, 1.53, 23.42}, respectively, and the mean rainfall in the low-precipitation bin and the three terciles for those two models are {0.0083, 0.10, 0.30, 0.93} and {0.0024, 0.14, 0.83, 3.71}, respectively, with all units in mm h^{-1}.

Comparing the terciles with the total tendencies in Figure 8, tercile 1 looks similar to the 1.0 E−1 bin for both models, as might be expected from the similar mean rain rates. Tercile 2 looks similar to the 3.0 E−1 bin for the 12 km *param* model and the mean rain rates are also the same, but for the 4 km *3Dsmag* model tercile 2 is signficantly different from the 3.0 E−1 bin and has some similarities to the 2.0 E+0 bin, as might be expected from the fact that all of its values lie in between the means of those two bins. Tercile 3 looks similar to 2.0 E+0 for the 4 km *3Dsmag* model, although its mean rain rate is significantly larger. For the 12 km *param* model, tercile 3 has a moistening profile that is lower in altitude and has significantly less low-level drying than the 2.0 E+0 bin, and its mean rain rate is only about half. Similar curves for the total temperature tendencies (not shown) are fairly similar to the three rainy bins in Figure 7 except that the tercile 3 heating rates look more similar to the 3.0 E−1 bin for the 12 km *param* model. Overall, it is clear that the moistening profiles and terciles are shifted to much lower rain rates for the 12 km *param* model than for the 4 km *3Dsmag* model. These curves support the idea that it should be more difficult for rainy regions to dry out at lower levels and for suppressed regions to moisten above the boundary layer in the 12 km param model relative to the 4 km 3Dsmag model, perhaps leading to preferred rain rates and insufficient convective transitions.

In any event, the different distributions of rainfall lead to different distributions of heating and moistening, which will be important to large scales. Whether or not these are also a cause of the difference in rainfall distribution is a more difficult question.

7. Summary and conclusions

We compare limited-area simulations of the tropical atmosphere over a very large domain at several different horizontal resolutions and with both parametrized and explicit convection versions for a 10 day MJO case study in April 2009. We then compare these simulations with TRMM precipitation observations (as well as other fields taken from ECMWF operational analyses and TMI satellite data) for the same domain and time period. The main finding of this article is that the explicit convection simulations have precipitation distributions that are much more similar to observations than the simulations with parametrized convection. This is true even though at least one of the simulations with explicit convection has a relationship between rainfall and lower-tropospheric moisture that is arguably even worse than the run with parametrized convection (and has a worse MJO, as discussed in Holloway, Woolnough, and Lister, 2012; pers. comm.).

The precipitation distribution in the parametrized convection run (shown at 12 km grid spacing, but similar to a run performed at 40 km grid spacing) exhibits relatively too much rainfall at light and moderate rain rates and too little rainfall at high rain rates. Indeed, while all of the explicit convection runs have probability densities similar to a power-law distribution across most of their range before decreasing exponentially at very high rain rates (similar to recent observational studies; DeMott *et al.*, 2007; Field and Shutts, 2009; Peters *et al.*, 2010), the 12 km *param* model with parametrized convection has a positive deviation from this type of power-law distribution, suggesting a 'preferred' scale of rainfall centred around 0.4 mm h^{-1} (10 mm day^{-1}). Rainfall rates around this value contribute more to the total rainfall in this model than higher or lower rates, unlike observations and explicit convection runs.

Although we do not show conclusive evidence for a specific mechanism that is lacking or incorrect in the parametrized convection run and would lead to this incorrect precipitation distribution, we do suggest several possible reasons for it. It is possible that the 12 km *param* model consumes CAPE and reaches radiative–convective equilibrium too quickly, preventing interactions between rainfall and circulations across many scales. For instance, Pearson *et al.* (2010) showed that explicit convection in a similar model configuration captured the observed progression of diurnal convection over West Africa from small to large scales, whereas parametrized convection models did not. There are also indications that the 12 km *param* model (compared with the explicit runs) lacks the ability to transition from suppressed to active conditions and vice versa, which would tend to maintain rainfall at an average, preferred rain rate.

Although the 4 km *3Dsmag* run appears to have a better, more realistic relationship between precipitation and moisture than the 12 km *param* run, this does not seem to be the main factor in determining the ability to simulate observed precipitation distributions because, as mentioned above, the 4 km *2Dsmag* run is able to simulate the observed precipitation distribution while having a very poor sensitivity of precipitation to moisture. Comparisons between the two 4 km runs and the 12 km *param* run suggest that there may be processes that require extremely high tropospheric humidity and/or result in very large upper-tropospheric heating and stabilization in order to produce very high rain rates for the 12 km *param* model, preventing those rates from occurring very often.

We hope that this study will encourage more comparisons between cloud-system-resolving simulations of large convective regimes, parametrized convection simulations and observations, to improve both parametrizations and high-resolution simulations with explicit convection.

Acknowledgements

We have used ECMWF operational analyses from the YOTC online archive. We thank Adrian Matthews for discussions

and for providing rainfall data in NetCDF format. Thanks to Thorwald Stein, Richard Allan and Jon Petch for useful comments. This work made use of the facilities of HECToR, the UK's national high-performance computing service, which is provided by UoE HPCx Ltd at the University of Edinburgh, Cray Inc and NAG Ltd, and funded by the Office of Science and Technology through EPSRC's High End Computing Programme. This research was carried out with funding from NERC grant NE/E00525X/1.

References

Allan RP, Soden BJ, John VO, Ingram W, Good P. 2010. Current changes in tropical precipitation. *Environ. Res. Lett.* **5**: 1–7.

Bretherton CS, Peters ME, Back LE. 2004. Relationships between water vapor path and precipitation over the tropical oceans. *J. Climate* **17**: 1517–1528.

Bretherton CS, Blossey PN, Khairoutdinov M. 2005. An energy-balance analysis of deep convective self-aggregation above uniform SST. *J. Atmos. Sci.* **62**: 4273–4292.

Chen SS, Zhao W, Donelan MA, Price JF, Walsh EJ. 2007. The CBLAST–Hurricane Program and the next-generation fully coupled atmosphere–wave–ocean models for hurricane research and prediction. *Bull. Am. Meteorol. Soc.* **88**: 311–317.

Ciesielski PE, Schubert WH, Johnson RH. 1999. Large-scale heat and moisture budgets over the ASTEX region. *J. Atmos. Sci.* **56**: 3241–3261.

Dai A, Trenberth KE. 2004. The diurnal cycle and its depiction in the Community Climate System Model. *J. Climate* **17**: 930–951.

Dai A, Lin X, Hsu KL. 2007. The frequency, intensity, and diurnal cycle of precipitation in surface and satellite observations over low- and mid-latitudes. *Clim. Dyn.* **29**: 727–744.

Davies T, Cullen MJP, Malcolm AJ, Mawson MH, Staniforth A, White AA, Wood N. 2005. A new dynamical core for the Met Office's global and regional modelling of the atmosphere. *Q. J. R. Meteorol. Soc.* **131**: 1759–1782.

DeMott CA, Randall DA, Khairoutdinov M. 2007. Convective precipitation variability as a tool for General Circulation Model analysis. *J. Climate* **20**: 91–112.

Derbyshire SH, Beau I, Bechtold P, Grandpeix JY, Piriou JM, Redelsperger JL, Soares PMM. 2004. Sensitivity of moist convection to environmental humidity. *Q. J. R. Meteorol. Soc.* **130**: 3055–3080.

Field PR, Shutts GJ. 2009. Properties of normalised rain-rate distributions in the tropical Pacific. *Q. J. R. Meteorol. Soc.* **135**: 175–186.

Grabowski WW. 2003. MJO-like coherent structures: Sensitivity simulations using the Cloud-Resolving Convection Parameterization (CRCP). *J. Atmos. Sci.* **60**: 847–864.

Gregory D, Rowntree PR. 1990. A mass flux convection scheme with representation of cloud ensemble characteristics and stability-dependent closure. *Mon. Weather Rev.* **118**: 1483–1506.

Guilyardi E, Wittenberg A, Fedorov A, Collins M, Wang C, Capotondi A, van Oldenborgh GJ, Stockdale T. 2009. Understanding El Niño in ocean–atmosphere general circulation models: Progress and challenges. *Bull. Am. Meteorol. Soc.* **90**: 325–340.

Hilburn KA, Wentz FJ. 2008. Intercalibrated passive microwave rain products from the unified microwave ocean retrieval algorithm (UMORA). *J. Appl. Meteorol. Clim.* **47**: 778–794.

Holloway CE, Neelin JD. 2009. Moisture vertical structure, column water vapor, and tropical deep convection. *J. Atmos. Sci.* **66**: 1665–1683.

Huffman GJ, Adler RF, Arkin P, Chang A, Ferraro R, Gruber A, Janowiak J, McNab A, Rudolf B, Shneider U. 1997. The Global Precipitation Climatology Project (GPCP) Combined Precipitation Dataset. *Bull. Am. Meteorol. Soc.* **78**: 5–20.

Huffman GJ, Adler RF, Bolvin DT, Gu GJ, Nelkin EJ, Bowman KP, Hoong Y, Stocker EF, Wolff DB. 2007. The TRMM Multisatellite Precipitation Analysis (TMPA): quasi-global, multiyear, combined-sensor precipitation estimates at fine scales. *J. Hydrometeorol.* **8**: 38–55.

Khairoutdinov MF, Krueger SK, Moeng CH, Bogenschutz PA, Randall DA. 2009. Large-eddy simulation of maritime deep tropical convection. *J. Adv. Model. Earth Syst.* **1**: 1–13.

Lean HW, Clark PA, Dixon M, Roberts NM, Fitch A, Forbes R, Halliwell C. 2008. Characteristics of high-resolution versions of the Met Office Unified Model for forecasting convection over the United Kingdom. *Mon. Weather Rev.* **136**: 3408–3424.

LeMone MA, Zipser EJ. 1980. Cumulonimbus vertical velocity events in GATE. Part I: Diameter, intensity and mass flux. *J. Atmos. Sci.* **37**: 2444–2457.

Lin JL, Mapes BE, Zhang M, Newman M. 2004. Stratiform precipitation, vertical heating profiles, and the Madden–Julian Oscillation. *J. Atmos. Sci.* **61**: 296–309.

Lin JL, Kiladis GN, Mapes BE, Weickmann KM, Sperber KR, Lin W, Wheeler MC, Schubert SD, Del Genio A, Donner LJ, Emori S, Gueremy JF, Hourdin F, Rasch PJ, Roeckner E, Scinocca JF. 2006. Tropical intraseasonal variability in 14 IPCC AR4 climate models. Part I: Convective signals. *J. Climate* **19**: 2665–2690.

Liu P, Satoh M, Wang B, Fudeyasu H, Nasuno T, Li T, Miura H, Taniguchi H, Masunaga H, Fu X, Annamalai H. 2009. An MJO simulated by the NICAM at 14- and 7-km resolutions. *Mon. Weather Rev.* **137**: 3254–3268.

Lock AP, Brown AR, Bush MR, Martin GM, Smith RNB. 2000. A new boundary layer mixing scheme. Part I: Scheme description and single-column model tests. *Mon. Weather Rev.* **128**: 3187–3199.

Love BS, Matthews AJ, Lister GMS. 2011. The diurnal cycle of precipitation over the Maritime Continent in a high-resolution atmospheric model. *Q. J. R. Meteorol. Soc.* **137**: 934–947.

Miura H, Satoh M, Nasuno T, Noda AT, Oouchi K. 2007. A Madden–Julian Oscillation event realistically simulated by a global cloud-resolving model. *Science* **318**: 1763–1765.

O'Gorman PA, Schneider T. 2009. The physical basis for increases in precipitation extremes in simulations of 21st-century climate change. *Proc. Natl Acad. Sci.* **106**: 14773–14777, DOI: 10.1073/pnas.0907610106.

Oouchi K, Noda AT, Satoh M, Miura H, Tomita H, Nasuno T, Iga S. 2009. A simulated preconditioning of typhoon genesis controlled by a boreal summer Madden–Julian Oscillation event in a global cloud-system-resolving model. *SOLA* **5**: 65–68.

Pearson KJ, Hogan RJ, Allan RP, Lister GMS, Holloway CE. 2010. Evaluation of the model representation of the evolution of convective systems using satellite observations of outgoing longwave radiation. *J. Geophys. Res.* **115**: D20206, DOI: 10.1029/2010JD014265.

Peters O, Neelin JD. 2006. Critical phenomena in atmospheric precipitation. *Nature Phys.* **2**: 393–396.

Peters O, Deluca A, Corral A, Neelin JD, Holloway CE. 2010. Universality of rain event size distributions. *J. Stat. Mech.* **2010**: P11030, DOI:10.1088/1742-5468/2010/11/P11030.

Roberts NM. 2003. '*The impact of a change to the use of the convection scheme to high-resolution simulations of convective events*, Technical Report 407, 30pp. UK Met Office: Exeter, UK.

Shige S, Takayabu YN, Tao WK, Shie CL. 2007. Spectral retrieval of latent heating profiles from TRMM PR data. Part II: Algorithm improvement and heating estimates over tropical ocean regions. *J. Appl. Meteorol. Clim.* **46**: 1098–1124.

Slingo JM, Sperber KR, Boyle JS, Ceron JP, Dix M, Dugas B, Ebisuzaki W, Fyfe J, Gregory D, Gueremy JF, Hack J, Harzallah A, Inness P, Kitoh A, Lau WKM, McAvaney B, Madden R, Matthews A, Palmer TN, Park TK, Randall D, Renno N. 1996. Intraseasonal oscillation in 15 atmospheric general circulation models: Results from an AMIP diagnostic subproject. *Clim. Dyn.* **12**: 325–357.

Sorooshian S, Hsu KL, Gao X, Gupta HV, Imam B, Braithwaite D. 2000. Evaluation of PERSIANN system satellite-based estimates of tropical rainfall. *Bull. Am. Meteorol. Soc.* **81**: 2035–2046.

Stephens GL, L'Ecuyer T, Forbes R, Gettlemen A, Golaz JC, Bodas-Salcedo A, Suzuki K, Gabriel P, Haynes J. 2010. Dreary state of precipitation in global models. *J. Geophys. Res.* **115**: D24211, DOI: 10.1029/2010JD014532.

Sun Y, Solomon S, Dai A, Portmann RW. 2006. How often does it rain? *J. Climate* **19**: 916–934.

Taniguchi H, Yanase W, Satoh M. 2010. Ensemble simulation of Cyclone Nargis by a global cloud-system-resolving model – modulation of cyclogenesis by the Madden–Julian Oscillation. *J. Meteorol. Soc. Jpn* **88**: 571–591.

Thayer-Calder K, Randall DA. 2009. The role of convective moistening in the Madden–Julian Oscillation. *J. Atmos. Sci.* **66**: 3297–3312.

Turner AG, Slingo JM. 2009. Uncertainties in future projections of extreme precipitation in the Indian monsoon region. *Atmos. Sci. Lett.* **10**: 152–158.

Waliser DE, Moncrieff M. 2008. '*The Year of Tropical Convection (YOTC) Science Plan: A joint WCRP–WWRP/THORPEX International Initiative*', Technical Report 1452, WMO/TD, WCRP 130, WWRP/THORPEX 9; 26pp. WMO: Geneva, Switzerland.

Wilcox EM, Donner LJ. 2007. The frequency of extreme rain events in satellite rain-rate estimates and an atmospheric general circulation model. *J. Climate* **20**: 53–69.

Wilson DR, Ballard SP. 1999. A microphysically based precipitation scheme for the UK Meteorological Office Unified Model. *Q. J. R. Meteorol. Soc.* **125**: 1607–1636.

Woolnough SJ, Blossey PN, Xu KM, Bechtold P, Chaboureau JP, Hosomi T, Iacobellis SF, Luo Y, Petch JC, Wong RY, Xie S. 2010. Modelling convective processes during the suppressed phase of a Madden–Julian oscillation: Comparing single-column models with cloud-resolving models. *Q. J. R. Meteorol. Soc.* **136**: 333–353.

Yanai M, Esbensen S, Chu JH. 1973. Determination of bulk properties of tropical cloud clusters from large-scale heat and moisture budgets. *J. Atmos. Sci.* **30**: 611–627.

Zhang GJ, McFarlane NA. 1995. Sensitivity of climate simulations to the parametrization of cumulus convection in the Canadian Climate Centre general circulation model. *Atmos.–Ocean.* **33**: 407–446.

Zhou YP, Tao WK, Hou AY, Olson WS, Shie CL, Lau KM, Chou MD, Lin X, Grecu M. 2007. Use of high-resolution satellite observations to evaluate cloud and precipitation statistics from cloud-resolving model simulations. Part I: South China Sea Monsoon Experiment. *J. Climate* **64**: 4309–4329.

